

Interfacial Magnetism in Manganite Superlattices

Kalpataru Pradhan and Arno P. Kampf

*Center for Electronic Correlations and Magnetism, Theoretical Physics III,
Institute of Physics, University of Augsburg, D-86135 Augsburg, Germany*

(Dated: December 3, 2024)

We use a two-orbital double-exchange model including Jahn-Teller lattice distortions, superexchange interactions, and long-range Coulomb (LRC) interactions to investigate the origin of magnetically disordered interfaces between ferromagnetic metallic (FM) and antiferromagnetic insulating (AFI) manganites in FM/AFI superlattices. The induced magnetic moment in the AFI layer varies non-monotonically with increasing AFI layer width as seen in the experiment. We provide a framework for understanding this non-monotonic behavior which has a one-to-one correspondence with the magnetization of the FM interface. The obtained insights provide a basis for improving the tunneling magnetoresistance in FM/AFI manganite junctions and suggest that the interface of a FM manganite joined with a non-magnetic insulating (NMI) oxide is locally antiferromagnetic.

The FM manganites have emerged as potential candidates for spintronics devices^{1,2} due to their high spin polarization^{3,4}. For the future generation of magnetic tunnel junctions (MTJs) artificial trilayers of insulating metal oxides sandwiched between FM manganites are currently designed. In MTJs a large tunneling magnetoresistance (TMR)⁵ is observed by switching the spin orientation in the FM leads from antiparallel to parallel configurations; the TMR is defined by the ratio $(R_{AP} - R_P)/R_P$ where R_{AP} and R_P are the resistances for antiparallel and parallel orientations, respectively⁶. Although SrTiO_3 is predominantly used as the insulator between $\text{La}_{0.67}\text{Sr}_{0.33}\text{MnO}_3$ (LSMO) layers, also other combinations of FM and NMI oxides (FM = LSMO, $\text{La}_{0.67}\text{Ca}_{0.33}\text{MnO}_3$ (LCMO); NMI = TiO_2 , LaAlO_3 , NdGaO_3) have also been tested for their performance^{7–10}.

TMR is a spin dependent process which critically depends on the magnetic and the electronic properties of the interface between FM manganites and the insulating material¹. In such a spin sensitive device it is required to have a structurally and magnetically well defined interface. It is an experimental fact that the magnetization of FM manganites decreases at the interface below its bulk value¹¹, the origin of which is not well understood. The reduction of the magnetization at the interface, usually referred to as the ‘magnetic dead layer’ (MDL)^{8,9} has an adverse effect on the TMR by decreasing the tunneling current, which by itself should be large for device applications.

The reduction of the magnetization has been attributed to phase separation, and/or electronic and magnetic reconstructions due to structural inhomogeneities at the interface. Unlike at the surface of FM manganites³ it is a difficult task to determine the electronic and structural changes at interfaces which are several nanometers below the surface. To minimize disorder and strain effects isostructural interfaces are favorable. In a different approach NMI barriers were replaced by AFI manganites^{12–15}. In the presence of a small external magnetic field not only the FM manganites align but there is a likely possibility that the magnetization in the

AFI layer also aligns along the FM leads^{12,14}. Specifically the relation between the magnetoresistance and the induced magnetic moment in the AFI barrier was established in $\text{LSMO}/\text{Pr}_{0.67}\text{Ca}_{0.33}\text{MnO}_3$ (PCMO)/LSMO superlattices¹⁶. The magnetic moment of the PCMO layers in the superlattice behaves non-monotonically with increasing PCMO layer width¹². Remarkably the magnetoresistance follows a very similar non-monotonic behavior. It is a priori not clear from the LSMO/PCMO/LSMO superlattices, if MDLs at the interface exist for different widths of the PCMO layers.

In this letter, we explore in detail the electronic and magnetic reconstructions of the FM/AFI superlattices at the electron density $n = 0.5$ for different widths of the AFI layers. Electrons are transferred from the FM to the AFI layers at the interface even though the initial electron density in the bulk materials are equal. The amount of electron transfer from the FM interfacial line depends upon the thickness of the AFI layer. We explain the non-monotonic behavior of the induced ferromagnetic moment in the AFI layer with increasing AFI layer width and establish explicitly a one-to-one correspondence between the induced magnetic moment in the AFI layer and the magnetization at the interface in the FM/AFI superlattices.

We consider a two-dimensional model Hamiltonian for manganite superlattices composed of alternating FM and AFI regions. The model and the method we employ have been elaborately discussed in Ref. 17. The model is given by

$$H = H_{FM} + H_{AFI} + H_{lrc}, \quad (1)$$

where both H_{FM} and H_{AFI} have the same reference Hamiltonian^{18–21}

$$H_{ref} = \sum_{\langle ij \rangle \sigma}^{\alpha\beta} t_{\alpha\beta}^{ij} c_{i\alpha\sigma}^\dagger c_{j\beta\sigma} - J_H \sum_i \mathbf{S}_i \cdot \boldsymbol{\sigma}_i + J \sum_{\langle ij \rangle} \mathbf{S}_i \cdot \mathbf{S}_j - \lambda \sum_i \mathbf{Q}_i \cdot \boldsymbol{\tau}_i + \frac{K}{2} \sum_i \mathbf{Q}_i^2 - \mu \sum_{i\alpha\sigma} c_{i\alpha\sigma}^\dagger c_{i\alpha\sigma}. \quad (2)$$

H_{ref} is constructed to qualitatively reproduce the phase diagram in the bulk limit^{21,22}. λ is the coupling

between the e_g electron and the Jahn-Teller phonons Q_i in the adiabatic limit, and J is the superexchange interactions between the t_{2g} spins \mathbf{S}_i . We treat \mathbf{S}_i and Q_i as classical²³ and set $|\mathbf{S}_i| = 1$. We also set the stiffness of Jahn-Teller modes $K = 1$ and the Mn-Mn hopping $t = 1$. t is the reference energy scale.

The Hund's coupling J_H , between \mathbf{S}_i and the e_g electron spin $\boldsymbol{\sigma}_i$, estimated to be 2 eV²⁵ in manganites, is much larger than t ($t \sim 0.2 - 0.5$ eV²⁴). For this reason we use the limit $J_H \rightarrow \infty$ ¹⁹. In an external magnetic field h we add a Zeeman coupling term $H_{mag} = -\mathbf{h} \cdot \sum_i \mathbf{S}_i$ to the Hamiltonian

The average electron density of the FM/AFI superlattice is fixed by choosing the same chemical potential μ at each site. The LRC part $H_{lrc} = \sum_i \phi_i n_i$ of the Hamiltonian controls the amount of charge transfer across the interface. Here a self-consistent solution of the Coulomb potentials $\phi_i = \alpha t \sum_{j \neq i} \frac{\langle n_j \rangle - Z_j}{|\mathbf{R}_i - \mathbf{R}_j|}$ is set up at the mean-field level²⁶⁻²⁸; for details see Ref. 17. $\alpha = e^2/\epsilon a t$ is the Coulomb interaction strength where ϵ and a are the dielectric constant and the lattice parameter, respectively. For the 2D case considered here α is approximately 0.1¹⁷.

We use the ‘traveling cluster approximation’ (TCA)²⁹ based Monte Carlo sampling technique. This method was already successfully applied in several earlier studies²⁰⁻²². At each system sweep, with the additional H_{lrc} term in the Hamiltonian, we solve for the Coulomb potentials ϕ_i self-consistently until the electron density n_i at each site is converged¹⁷. All physical quantities are averaged over the results for ten different ‘samples’ where each sample denotes a different initial realization of the classical variables.

Here we analyze specifically superlattices composed of FM and AFI manganites of equal electron density $n = 0.5$. We use the typical value $J = 0.1$ ^{21,30} for both the FM and the AFI manganites and differentiate between a FM and an AFI phase by varying λ . For the parameters $J = 0.1$ and $n = 0.5$, the groundstate is a FM for $\lambda \equiv \lambda_M = 1.0$ while it is an AFI for $\lambda \equiv \lambda_I \geq 1.6$. The AFI phase at $n = 0.5$ is a charge and orbital ordered CE phase²¹. The density of states is finite for the FM phase while it is gapped at the Fermi level for the AFI phase; charge transfer from the FM to the AFI side is expected when the FM and the AFI are joined together.

Two types of FM/AFI superlattices are shown schematically in Fig.1; w denotes the width of the AFI spacer. Periodic boundary conditions in both directions ensures that the superlattice structures are composed of alternating FM and AFI layers. The type I superlattice is considered in the following discussions while results for the type II superlattice are discussed in the concluding paragraphs.

Different combinations of electron-phonon couplings ($\lambda_M = 1.0$, $\lambda_I = 1.6 - 2.0$) are considered first in the absence of LRC intractions $\alpha = 0$. To start with we discuss the results for $\lambda_I = 1.65$ (see Fig.2(a)), for which the ferromagnetic structure factor $\langle S_I(\mathbf{0}) \rangle$ behaves non-monotonically with increasing AFI layer width, where

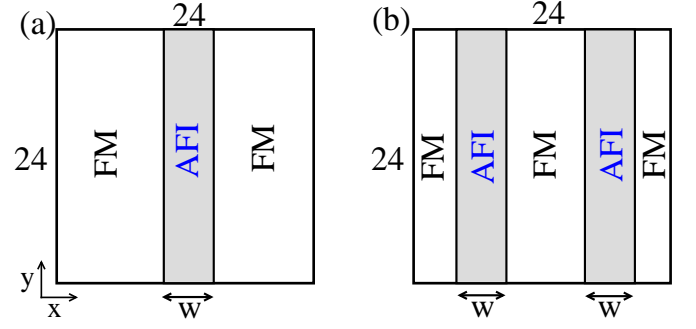


FIG. 1: (Color online) Schematic view of the FM/AFI superlattice on a 24×24 lattice. (a) Type I : one AFI layer (b) type II: two AFI layers.

$S_I(\mathbf{q}) = \frac{1}{N_I^2} \sum_{ij \in AFI} \mathbf{S}_i \cdot \mathbf{S}_j e^{i\mathbf{q} \cdot (\mathbf{r}_i - \mathbf{r}_j)}$ and the angular bracket denotes the average over thermal equilibrium configurations combined with an additional average over ten different ‘samples’. The induced magnetization in the AFI layer is small for $w = 1$, nearly equal to 1 (all the t_{2g} spins are fully ordered) for $w = 2$, and rapidly decreases for $w > 7$.

The averaged z component of the t_{2g} spins $\langle S_{zI} \rangle$ in the AFI layer for $\lambda_I = 1.65$ is similarly non-monotonic as $\langle S_I(\mathbf{0}) \rangle$ as shown in Fig.2(b). We also calculate the local staggered charge order by $\langle CO_I \rangle = \frac{1}{N_I} \sum_{i \in AFI} \langle n_i \rangle e^{i(\pi, \pi) \cdot \mathbf{r}_i}$ where i denotes lattice sites in the AFI layer with position \mathbf{r}_i . $\langle CO_I \rangle$, shown in Fig.2(b), remains small for $w \leq 7$ and starts to rise for $w > 7$. The decrease in the magnetization accompanied by the emerging charge order indicate that the AFI layer gradually returns to the bulk AFI state with increasing w .

$\langle S_I(\mathbf{0}) \rangle$ for different λ_I values also varies non-monotonically with increasing width of the AFI layer except for $\lambda_I = 2.0$. The induced magnetic moment for $w > 2$ decreases more rapidly for larger electron-phonon coupling λ_I . The AFI layer recovers the AF, charge ordered state at a smaller width w for larger λ_I . This is why it is possible to magnetize only 2 lines of the AFI layer for $\lambda_I = 1.8$ while for $\lambda_I = 2.0$ the induced magnetic moment remains very small in the AFI layer irrespective of its width.

In order to understand the non-monotonic behavior we specifically choose $w = 1$ and $w = 9$ for which $\langle S_I(\mathbf{0}) \rangle$ is small. To start with we analyze the magnetization profile across the interface by calculating average magnetization for each line of the superlattice $\langle S_z(x) \rangle$ for transverse coordinate x . $\langle S_z(x) \rangle$, in Fig.2(c), decreases for $x = 11-15$ for $w = 9$, i.e. in the center lines of the AFI layer, which implies that the induced ferromagnetic moment in the AFI layer is confined to the near vicinity of the interface. The relation between the induced magnetization and the line-averaged electron density $\langle n(x) \rangle$ becomes evident in Fig.2(d). $\langle n(x) \rangle$ for the interfacial line on the FM side, named as FM interfacial line, decreases while the AFI interfacial line increases from the initial electron density

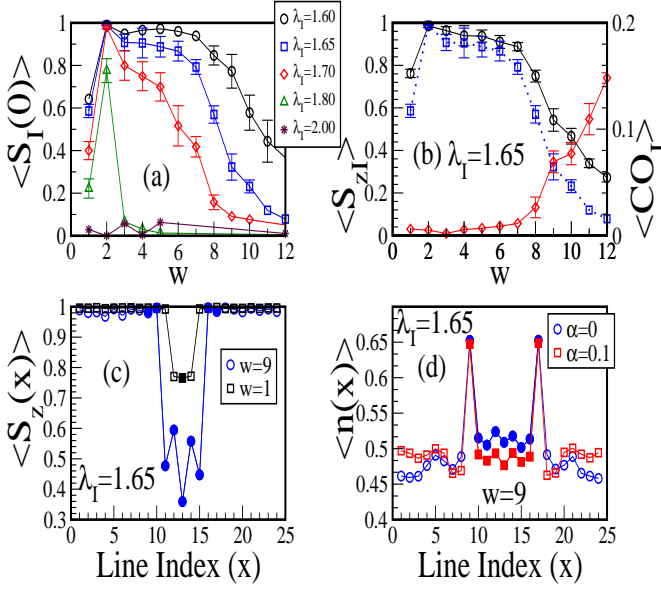


FIG. 2: (Color online) (a) Ferromagnetic structure factor $\langle S_I(\mathbf{0}) \rangle$ in the AFI layer for $w = 1 - 12$ at $T = 0.01$ ($\lambda_M = 1.0$ and $\lambda_I = 1.6 - 2.0$). (b) $\langle S_{zI} \rangle$ and $\langle COI \rangle$ (see text) in the AFI layer for $\lambda_M = 1.0$ and $\lambda_I = 1.65$. $\langle S_I(\mathbf{0}) \rangle$ is also included as the dotted line. (c) Line averaged z component of the t_{2g} spins $\langle S_z(x) \rangle$ for $w = 9$ and $w = 1$, (d) line averaged electron density $\langle n(x) \rangle$ for $w = 9$ with ($\alpha = 0.1$) and without ($\alpha = 0.0$) LRC interactions. In (c) and (d) open and closed symbols are from lines in the FM and the AFI layers, respectively.

0.5 to ~ 0.65 . The induced ferromagnetic moment for the lines $x = 9$ and 17 is therefore due to the enhanced electron density and the spin bias from the ferromagnetic metal. In fact, for the parameters $J = 0.1$, $n = 0.65$, and $\lambda_I = 1.65$ the groundstate of the bulk system is a FM. The magnetization in the line $x = 10$ (16) is induced by the fully magnetized line $x = 9$ (17). The spin bias from the ferromagnetic metal is important for the induction of a ferromagnetic moment in the AFI interfacial lines. The induced magnetization in the AFI layer is very small irrespective of the AFI layer width where the FM interfacial lines are magnetically disordered¹⁷.

The direction of electron transfer is from the FM to the AFI layer as anticipated earlier. Sufficiently far away from the interface the average electron density must return to the initial electron density $n = 0.5$, which however is not fully accomplished for $w = 9$ and $\alpha = 0$. But with the additional LRC interaction $\langle n(x) \rangle$ indeed gradually returns to the initial electron density (see Fig.2(d)). For $\alpha = 0.1$ the average electron densities are clearly higher (lower) in the FM (AFI) layers as compared to $\alpha = 0$. In the FM/AFI superlattices, where the constituent FM and AFI manganites have the same initial electron density, the LRC interaction reduces the critical width, beyond which $\langle S_I(\mathbf{0}) \rangle$ starts to decrease¹⁷. Remarkably, $\langle n(x) \rangle$ at the FM interfacial lines is largely unaltered by the LRC interactions.

The line averaged $\langle S_z(x) \rangle$ for $w = 1$ is also shown in

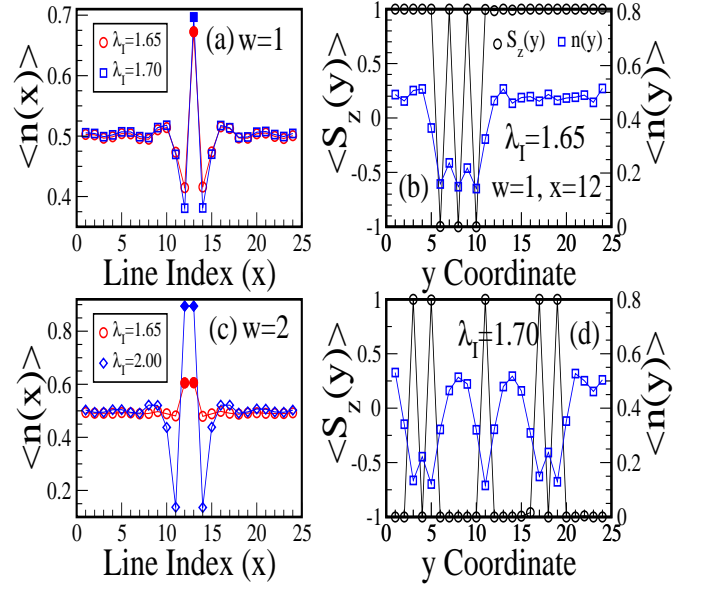


FIG. 3: (Color online) Line averaged electron density $\langle n(x) \rangle$ for (a) $w = 1$, (c) $w = 2$. The z component of the t_{2g} spins $\langle S_z(y) \rangle$ and $\langle n(y) \rangle$ for each site of the FM interfacial line $x = 12$ for $w = 1$ using (b) $\lambda_I = 1.65$ and (d) $\lambda_I = 1.70$. Legends in (b) and (d) are the same. Open and closed symbols in (a) and (c) are from lines in the FM and the AFI layers, respectively.

Fig.2(c). But in contrast to the AFI layer width $w = 9$, $\langle S_z(x) \rangle$ in the FM interfacial line decreases for $w = 1$. The difference results from the decrease in the electron density for $w = 1$ in the FM interfacial line as shown in Fig.3(a). The spin pattern in the interfacial line decomposes into FM and G-type AF regions. This is shown in Fig.3(b) which displays the averaged z components of the t_{2g} spins $\langle S_z(y) \rangle$ for each site of the FM interfacial line $x = 12$ for one selected 'sample'.

The averaged electron density at the FM interfacial line is smaller for $\lambda_I = 1.70$ as compared to $\lambda_I = 1.65$ as shown in Fig.3(a). For this reason the G-type AF regions in the FM interfacial line are more pronounced for $\lambda_I = 1.70$ (see Fig.3(d)). The electron densities and the z components of the t_{2g} spins at each site in the FM/AFI superlattice are shown in Fig.4 for $w = 1$. The magnetic and the electronic profile of both FM interfacial lines are similar to each other on both sides of the AFI line. The magnetic profile of the AFI line is tied to the profile of the FM interfacial lines while the electron density of the sites in the AFI layer is enhanced to ~ 0.7 .

With increasingly larger values of λ_I the magnetization of the FM interfacial line decreases due to the enhanced G-type correlations for $w = 1$. This establishes the crucial relation between the magnetization at the FM interfacial line and the induced magnetic moment in the AFI layer. This is in general true for any width w . So the non-monotonic behavior of $\langle S_I(\mathbf{0}) \rangle$ in Fig.2(a) implies that the FM interfacial line remains ferromagnetic for $w = 2$. For $w = 2$ the decrease in the electron density

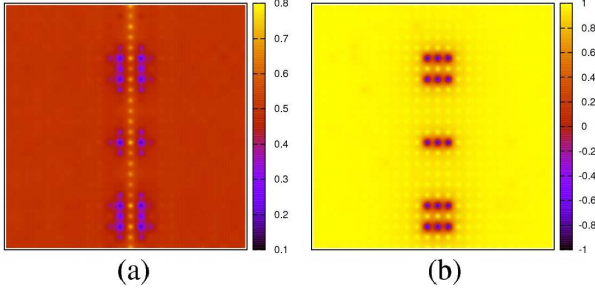


FIG. 4: (Color online) (a) The electron densities and (b) the z components of the t_{2g} spins for each site on a 24×24 superlattice at $T = 0.01$ with the AFI layer width $w = 1$ ($\lambda_M = 1.0$ and $\lambda_I = 1.7$).

in the FM interfacial line (see Fig.3(c), $\lambda_I = 1.65$) is very small as compared to $w = 1$, and these lines therefore remain ferromagnetic. The competition between FM and G-type AF spin patterns at the interface is controlled by the double-exchange energy gain due to the induced magnetic moment in the AFI layer.

At large electron-phonon couplings $\lambda_I \gtrsim 2.0$ electrons are site-localized due to strong lattice distortions; this decreases the double-exchange energy gain from induced ferromagnetic moments which are hence absent in the AFI layer (see Fig.2(a)) irrespective of the AFI layer width. For this reason G-type spin patterns are more prominent at the FM interfacial lines and $\langle n(x) \rangle$ in the FM interfacial line decreases considerably (see e.g. Fig.3(c) for $w = 2$ and $\lambda_I = 2.0$). These results suggest that also in FM/NMI superlattices local AF correlations may emerge in the FM interfacial line and the magnetization at the interface is wiped out due to the decrease in the electron density at the interface^{8,9}.

In the type I FM/AFI superlattices the spins in the FM leads are aligned in the same direction due to the periodic boundary conditions; this set up mimics the experimental situation in which the FM layers of the superlattice are aligned by an external magnetic field. Specifically we have designed the type II superlattice where two AFI layers instead of one are considered as shown in Fig.1(b) to represent more closely the experimental setup. The magnetizations in the left and the right FM layers are aligned parallel while the middle FM layer is free to choose its spin direction. A small external magnetic field h is applied to align all the FM layers in the same direction. Fig.5(a) shows the line averaged $\langle n(x) \rangle$ vs. line index x for $w = 1$, $\lambda_I = 1.8$, and $h = 0.002$. In Fig.5(b), we plot the averaged $\langle S_{zI} \rangle$ in the AFI layers along with averaged z component of the t_{2g} spins in the FM interfacial lines $\langle S_z(IL) \rangle$ for the same magnetic field. The magnetization of the FM interfacial line follows a non-monotonic behavior similar to the induced magnetic moments in the AFI layer. The dc limit of the longitudinal conductivity σ_{dc} , also displayed in Fig.5(b), as obtained from the Kubo-Greenwood formula^{31,32}, follows the same trend with increasing AFI layer width w . It is the combi-

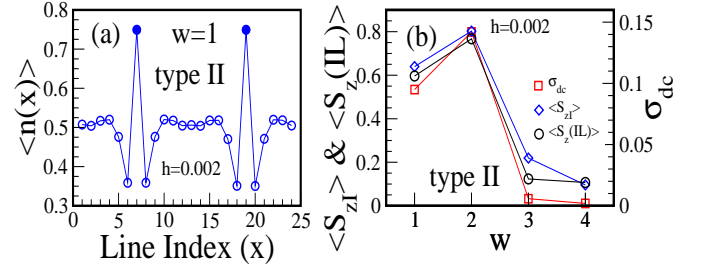


FIG. 5: (Color online) Type II FM/AFI superlattice ($\lambda_M = 1.0$ and $\lambda_I = 1.8$): (a) Line averaged z component of the t_{2g} spins $\langle S_z(x) \rangle$ for $w = 1$. (b) $\langle S_{zI} \rangle$, $\langle S_z(IL) \rangle$ (see text) and the dc conductivity (in units of $\pi e^2 / \hbar a$ where a is the lattice spacing, see Ref. 32) at $T = 0.01$ for different AFI layer widths w . An external magnetic field $h = 0.002$ is applied to align the FM layers.

nation of the induced magnetic moment in the AFI layer and the magnetization of the FM interfacial lines which enhances the conductivity.

In the type II set up the TMR may be calculated by fixing the spins of the middle FM layer in the direction opposite to that of the left and right FM layers. However in the limit $J_H \rightarrow \infty$ adopted here where the spins of the mobile e_g electrons are perfectly aligned along the local t_{2g} spin direction the dc conductivity (resistivity) for this set up is zero (infinity). In the experiments the resistivity is large but finite in the antiparallel configuration of the FM layers. The decrease (increase) of the resistivity (conductivity) in the parallel configuration of the FM layers will therefore enhance the TMR.

In conclusion, our 2D model calculations provide a framework to explain the origin of the MDL at the FM interface in FM/Insulator superlattices. The magnetization of the interfacial lines of the FM layers is determined by the amount of electron transfer from the FM interfacial lines to the AFI layer. The decrease in the magnetization of the FM interface, when joined with a NMI oxide is due to the decrease in the electron density at the interfacial lines as a result of the charge transfer across the interface. The amount of transferred charge is limited in a scenario for which instead AFI layers are sandwiched between FM layers, since inducing ferromagnetic moment in the AFI layer requires to control the charge transfer. But even in such a FM/AFI superlattices, the MDL is absent only for a specific range of AFI layer widths, because the induced magnetic moment in the AFI layer varies non-monotonically with the AFI layer width¹². AFI layer materials, for which the induced ferromagnetic moment is large, are suitable candidates for MTJs to enhance the TMR. The MDL at the interface in a FM/NMI junction may in fact be minimized by the insertion of an intervening AFI layer. In such a setup, the width of the AFI layer has to be chosen such that the AFI layer is maximally polarized along the direction of the magnetization in the FM layers due to charge transfer.

This work was supported by the DFG through TRR80.

REFERENCES

- ¹ J. M. De Teresa, A. Barthélémy, A. Fert, J. P. Contour, F. Montaigne, and P. Seneor, *Science* **286**, 507 (1999).
- ² M. Bibes and A. Barthélémy, *IEEE Trans. Electron Devices* **54**, 1003 (2007).
- ³ J.-H. Park, E. Vescovo, H.-J. Kim, C. Kwon, R. Ramesh, and T. Venkatesan, *Nature (London)* **392**, 794 (1998).
- ⁴ *Colossal Magnetoresistive Oxides*, edited by Y. Tokura (Gordon and Breach, New York, 2000).
- ⁵ M. Bowen, M. Bibes, A. Barthélémy, J. P. Contour, A. Anane, Y. Lemaître, and A. Fert, *Appl. Phys. Lett.* **82**, 233 (2003).
- ⁶ M. Julliere, *Phys. Lett. A* **54**, 225 (1975).
- ⁷ J. Z. Sun, W. J. Gallagher, P. R. Duncombe, L. Krusin-Elbaum, R. A. Altman, A. Gupta, Yu Lu, G. Q. Gong, and Gang Xiao, *Appl. Phys. Lett.* **69**, 3266 (1996).
- ⁸ J. Z. Sun, D. W. Abraham, R. A. Rao, and C. B. Eom, *Appl. Phys. Lett.* **74**, 3017 (1999).
- ⁹ M. Bibes, L. Balcells, S. Valencia, J. Fontcuberta, M. Wojcik, E. Jedryka, and S. Nadolski, *Phys. Rev. Lett.* **87**, 067210 (2001).
- ¹⁰ V. Garcia, M. Bibes, A. Barthélémy, M. Bowen, E. Jacquet, J. P. Contour, and A. Fert, *Phys. Rev. B* **69**, 052403 (2004).
- ¹¹ J. W. Freeland, J. J. Kavich, K. E. Gray, L. Ozuyzer, H. Zheng, J. F. Mitchell, M. P. Warusawithana, P. Ryan, X. Zhai, R. H. Kodama, and J. N. Eckstein, *J. Phys.: Condens. Matter* **19**, 315210 (2007).
- ¹² D. Niebieskikwiat, L. E. Hueso, J. A. Borchers, N. D. Mathur, and M. B. Salamon, *Phys. Rev. Lett.* **99**, 247207 (2007).
- ¹³ R. Cheng, K. Li, S. Wang, Z. Chen, C. Xiong, X. Xu, and Y. Zhang, *Appl. Phys. Lett.* **72**, 2475 (1998).
- ¹⁴ H. Li, J. R. Sun, and H. K. Wong, *Appl. Phys. Lett.* **80**, 628 (2002).
- ¹⁵ M. Jo, M. G. Blamire, D. Ozkaya, and A. K. Petford-Long, *J. Phys.: Condens. Matter* **15**, 5243 (2003).
- ¹⁶ D. Niebieskikwiat, L. E. Hueso, N. D. Mathur, and M. B. Salamon, *Appl. Phys. Lett.* **93**, 123120 (2008).
- ¹⁷ K. Pradhan and A. P. Kampf, *Phys. Rev. B* **87**, 155152 (2013).
- ¹⁸ S. Yunoki, T. Hotta, and E. Dagotto, *Phys. Rev. Lett.* **84**, 3714 (2000).
- ¹⁹ E. Dagotto, T. Hotta, and A. Moreo, *Phys. Rep.* **344**, 1 (2001).
- ²⁰ S. Kumar, A. P. Kampf, and P. Majumdar, *Phys. Rev. Lett.* **97**, 176403 (2006).
- ²¹ K. Pradhan, A. Mukherjee, and P. Majumdar, *Phys. Rev. Lett.* **99**, 147206 (2007).
- ²² K. Pradhan, A. Mukherjee, and P. Majumdar, *Europhys. Lett.* **84**, 37007 (2008).
- ²³ E. Dagotto, S. Yunoki, A. L. Malvezzi, A. Moreo, J. Hu, S. Capponi, D. Poilblanc, and N. Furukawa, *Phys. Rev. B* **58**, 6414 (1998).
- ²⁴ Z. Popovic and S. Satpathy, *Phys. Rev. Lett.* **88**, 197201 (2002).
- ²⁵ Y. Okimoto, T. Katsufuji, T. Ishikawa, A. Urushibara, T. Arima, and Y. Tokura, *Phys. Rev. Lett.* **75**, 109 (1995).
- ²⁶ S. Okamoto and A. J. Millis, *Phys. Rev. B* **70**, 075101 (2004).
- ²⁷ S. Yunoki, A. Moreo, E. Dagotto, S. Okamoto, S. S. Kancharla, and A. Fujimori, *Phys. Rev. B* **76**, 064532 (2007).
- ²⁸ J. Salafranca, M. J. Calderon, and L. Brey, *Phys. Rev. B* **77**, 014441 (2008).
- ²⁹ S. Kumar and P. Majumdar, *Eur. Phys. J. B* **50**, 571 (2006).
- ³⁰ T. G. Perring, G. Aeppli, Y. Moritomo, and Y. Tokura, *Phys. Rev. Lett.* **78**, 3197 (1997).
- ³¹ G. D. Mahan, *Quantum Many Particle Physics* (Plenum Press, New York, 1990).
- ³² S. Kumar and P. Majumdar, *Eur. Phys. J. B* **46**, 237 (2005).